

Flexible Composites with Programmed Electrical Anisotropy Using Acoustophoresis

Drew S. Melchert^a, Rachel R. Collino^b, Tyler R. Ray^c, Neil Dolinski^a, Leanne Friedrich^a, Matthew R. Begley^a, Daniel S. Gianola^a

^aMaterials Department, Engineering II Building 1355, University of California Santa Barbara, Santa Barbara, CA, 93106, USA

^bMST-7 Engineered Materials, Division of Materials Science and Technology, Los Alamos National Lab, Los Alamos, NM 87545

^cDepartment of Mechanical Engineering, 2540 Dole St, University of Hawai'i at Manoa, Honolulu, HI 96822

Abstract

A single-step process that utilizes acoustophoresis to modulate the electrical properties of composites is developed to address the demand for 3-D printing multifunctional materials. Here, acoustic fields assemble conductive particles into networks within polymer matrices, whose configuration is modulated prior to curing to produce 2-D conductive, 1-D conductive, or insulating materials on-demand, all using the same precursor ink. These variously patterned materials, used as electrical interconnects, are demonstrated to yield discrete, useful outputs from an electrical circuit. Furthermore, patterning efficient percolated networks in this way increases conductivity an order of magnitude over conventional dispersed-fiber composites, which rely on inefficient stochastic networks, to >5000 S/m bulk conductivity (2.6v% silver-coated fibers; 97% network efficiency). Similarly, these efficient networks require an order of magnitude lower particle loading than dispersed-fiber composites, improving printability and allowing versatile orthogonal control of other properties. As a demonstration of this multifunctional control, conductive elastomeric composites made with this method are demonstrated to withstand >500 bending cycles to a radius of 0.7 mm without losses in conductivity. This technology demonstrates a novel approach to modulating material properties via on-the-fly microstructure control to pave the way for 3D printing components with embedded electrical circuits or other spatially modulated properties.

Keywords: acoustophoresis, composite, conductive, flexible, 3D printing

Tremendous progress in 3D printing in recent years has created a demand for multifunctional printable materials that has yet to be satisfied. Currently, adding electronic, thermal, or flexible elements into 3D-printed components introduces costly and time consuming post-printing steps [1]. Developing a viable single-step process for printing components with integrated functional elements will enable significant advances in applications like soft robotics [2], wearable electronics [3], thermal management devices [4], etc.

To address this demand, a promising approach is to print components using polymer matrix composites with spatially modulated properties. Composite materials have a wide range of useful properties, such as high stiffness [5, 6], high electrical conductivity [7], and high thermal conductivity [8], as well as combinations of multiple of these properties. In addition, when the distribution of filler particles is altered during the 3D printing process

[9], these properties can be modulated spatially throughout the printed component to form integrated functional elements in programmed configurations. A particularly useful application of this technology is producing components with embedded electrical interconnects, which would eliminate expensive and time-consuming wiring steps [1, 7].

A promising approach to engineering the configuration of filler particles in composites is field-assisted assembly, in which external fields assemble filler particles into functional structures within the material before curing, thereby modulating material properties [10]. This approach avoids filler particle size and resolution limitations, material compatibility issues, and the high production time, complexity, and cost associated with multiple-material printing [10, 11, 12, 13, 14]. Acoustophoresis, also called acoustic focusing, is a field-assisted assembly technique that employs pressure fields to rotate and trans-

Email addresses: dsmelchert@ucsb.edu (Drew S. Melchert), begley@engr.ucsb.edu (Matthew R. Begley), gianola@ucsb.edu (Daniel S. Gianola)

late particles of nearly any material within a fluid, with the potential to assemble user-specified 3D patterns of particles [15, 16]. Acoustophoresis has a distinct advantage over electromagnetic field assisted assembly, which can only handle conductive or magnetic particles and can only rotate particles [17, 18, 19], or hydrodynamic shear alignment, which can only effectively rotate particles [5, 14, 20]. Another advantage of acoustic focusing is its speed and scalability: it assembles μm - to mm -size structures in seconds [21, 22], in contrast to self-assembly which is limited by diffusion rates and is prohibitively slow to assemble $>10 \mu\text{m}$ structures. Though currently used primarily for cell sorting and other biological characterization [23], acoustic focusing can be combined with direct ink writing [21, 24, 9] or stereolithography [16] to enable integration of functional particle structures into 3D-printed components.

Here we develop a strategy for modulating electrical conductivity and transport anisotropy in composite materials using acoustic focusing to pave the way for printing of components with integrated electrical circuits. We demonstrate that the electrical behavior of these patterned composites can be switched between conductive and insulating, and additionally between isotropic and anisotropic conductive, all on-the-fly using the same precursor ink. In addition, composites patterned with acoustic focusing require an order of magnitude lower particle concentration to reach the same conductivity of conventional dispersed-fiber composites, which here exceeds 5000 S/m. Finally, we demonstrate that these patterned composites can be used as durable flexible conductors, with constant conductivity over 500 cycles to 0.7 mm bending radius.

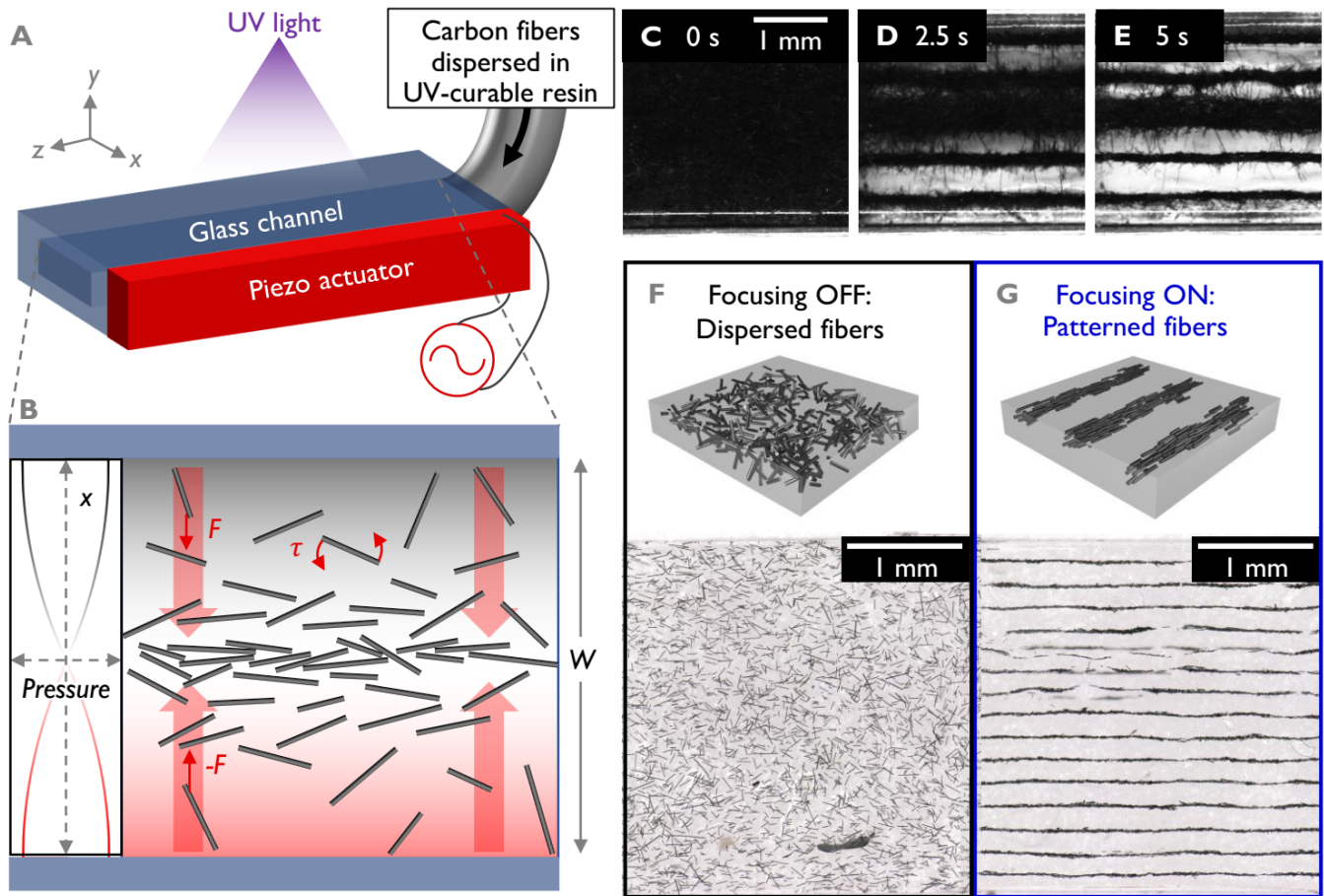


Figure 1: **A** Schematic of acoustic focusing device. **B** Diagram of forces aligning and pushing fibers to the center of a channel as the result of a standing pressure half-wave. **C,D,E** Time-lapse of fibers patterned into parallel bundles by acoustic focusing in photopolymer resin, reaching equilibrium positions after 5-6 seconds. **F** Illustration and micrograph of an unpatterned composite with carbon fibers dispersed in acrylate resin (0.36% carbon fiber). **G** Illustration and micrograph of a patterned carbon-fiber in acrylate composite (0.36% carbon fiber) fabricated with acoustic focusing.

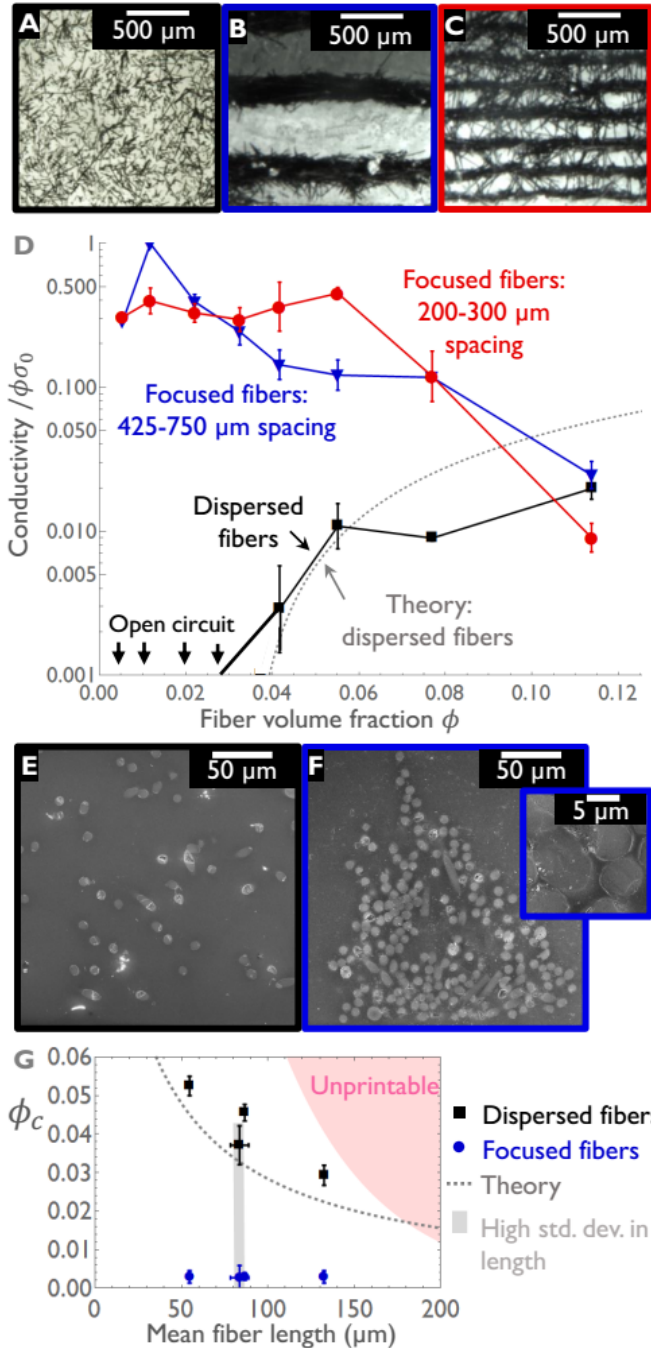


Figure 2: **A** Micrograph of a 0.5v% composite made without acoustic focusing. **B** Micrographs of 2.6v% composites made with acoustic focusing with 200-300 μm focused) bundle spacing and **C** with 425-600 μm spacing. **D** Electrical conductivity of carbon-fiber composites made with and without acoustic focusing. Conductivity is normalized by the conductivity of the fibers, σ_0 , and the volume fraction ϕ to give the fraction of fibers in the composite that contribute to the conductive network. Error bars represent the standard deviation of trials on at least three samples. **E** SEM images of cross-sections of a 2.6% carbon-fiber composites with dispersed fibers (insulating) and **F** focused fiber bundles spaced 500 μm apart (conductive). **G** The percolation threshold ϕ_c , at which electrical behavior transitions from insulating to conductive, for composites made with four fiber length distributions. The “unprintable” region indicates approximately which volume fractions and fiber lengths clog the devices. Composites in **A-D** have the fiber length distributions with high standard deviation highlighted in grey in **G**.

Our approach utilizes pressure fields to manipulate particles suspended in an ink in a printing nozzle. Pressure fields are generated by resonating the channel walls of the glass nozzle with a piezoelectric actuator [25, 26, 27], as shown in Figure 1A. When the walls are oscillated at the channel’s fundamental resonant frequency, $f_1 = c/2W$ where c is the speed of sound of the ink and W is the channel width, a sinusoidal pressure field $P_1 \propto \sin(2\pi x/W)$ is established. Particles are pushed to the nearest of n low-pressure nodes spaced equally across the nozzle, as shown in Fig. 1. A more thorough treatment of the acoustic forces on rod-like particles is given in [SI].

To demonstrate the spatial programming of electrical conductivity, we employ a two-component system of carbon fibers or silver-coated glass fibers in acrylate photopolymer matrices. First, composites were UV-cured without acoustic focusing, fibers uniformly dispersed, as shown in Fig. 2A. The unfocused composites are insulating at fiber volume fractions ϕ below 3.3%, resulting in an open-circuit measurement (Fig. 2). Above 3.3%, these composites have low conductivity (< 1 S/m), with around 1% of the fibers contributing to the conductive network. This transition from insulating to conductive behavior at $\phi = 3.3\%$ is termed the percolation threshold ϕ_c , given by $\phi_c = 1/(\pi/2a + 2a + 3 + \pi) = 3.3\%$, where $a = l/d$ is the aspect ratio of the fibers [28].

Below this threshold, too few particles are in contact to form a continuous network, so that charge transport across the material is blocked by regions of insulating matrix material. Above ϕ_c , however, a continuous conductive network supports charge transport across the material. Percolation theory models the conductivity of two-phase composite materials as $\sigma = \sigma_0(\phi - \phi_c)^2$ for $\phi > \phi_c$ [28], where σ_0 is a fitting parameter that gives the particle and contact resistance [29], and the exponent value of 2 describes a 3D network of low aspect-ratio ($a < 100$) fibers. Conductivity is expected to be overestimated by this model due to hydrodynamic alignment of fibers during loading of the channel [28]. The particle and contact resistance σ_0 for carbon fibers is 1000 S/m, two orders of magnitude lower than the conductivity of the fibers, indicating that there is significant contact resistance between the carbon fibers.

Next, using an identical precursor composition, the fibers are focused into bundles using acoustophoresis before the composite is UV-cured, yielding patterned composites as shown in 2B,C. The focused bundle spacing is equal to the half-wavelength of the pressure field: focusing at $f \approx 1.1$ MHz yields spacing $\lambda/2 = 200$ -300 μm; focusing at $f \approx 3.3$ MHz yields $\lambda/2 = 425$ -750 μm [SI]. With acoustic focusing turned on, the conductivity of the patterned carbon-fiber composites is dramatically

higher than the unpatterned composites, as shown in Fig. 2D. Below the percolation threshold ϕ_c , where the unpatterned composites are insulating, the composites made with acoustic focusing have high conductivity, with up to 98% of the fibers (by volume) contributing to the conductive network. At volume fractions up to 8%, the conductivity of the acoustically patterned composites is at least an order of magnitude higher than that of unpatterned percolated composites made with the same precursor ink.

This high conductivity is due to high contact efficiency between fibers, as revealed by cross-sectional SEM images of focused fiber bundles, Fig. 2F. The (non-normalized) conductivity of composites with 1-10% carbon fiber loading is roughly constant at 10 S/m (Ohmic [SI]); for silver-coated glass fibers (Fig. 3), conductivity is $>5,000$ S/m. These values are an order of magnitude higher than those reached in dispersed-fiber composites at 12%, above which the nozzle clogs immediately. Conductivity is measured parallel to the focused lines, and calculated using the volume of the entire composite.

The maximum in normalized conductivity of 98% at $\phi = 1.2\%$ is a result of fibers preferentially stacking end-on-end due to scattering forces in the x -direction [24], an optimal contact configuration. At the lowest extreme, 0.4%, however, some focused lines break continuity, so

that conductivity drops (see Fig. 1G). At volume fractions above 1.2%, the contact efficiency of 200-300 μm spaced bundles decreases as some fibers are oriented radially outward from the bundles, and remains roughly constant for the more widely 425-750 μm spaced lines. At 12%, the maximum printable loading before channels clogged during loading, the normalized conductivity decreases to 1-5% because scattered-wave interactions [16] and distorted pressure fields at such high solid content greatly decrease the degree of fiber compaction and alignment [SI].

Notably, conductivity in patterned composites is invariant from 1-10%, in contrast to the strong scaling in unpatterned composites. Additionally, the critical volume fraction for conductivity in patterned composites is independent of fiber length, and an order of magnitude lower at 0.36% than the unpatterned composites, as shown in Fig. 2G. Again, this is not observed in the unpatterned composites, which have percolation threshold strongly dependent on fiber length [28]. This tolerance to fiber length and loading changes suggests freedom to orthogonally control other material properties, like stiffness, strength, or thermal conductivity, while maintaining high conductivity.

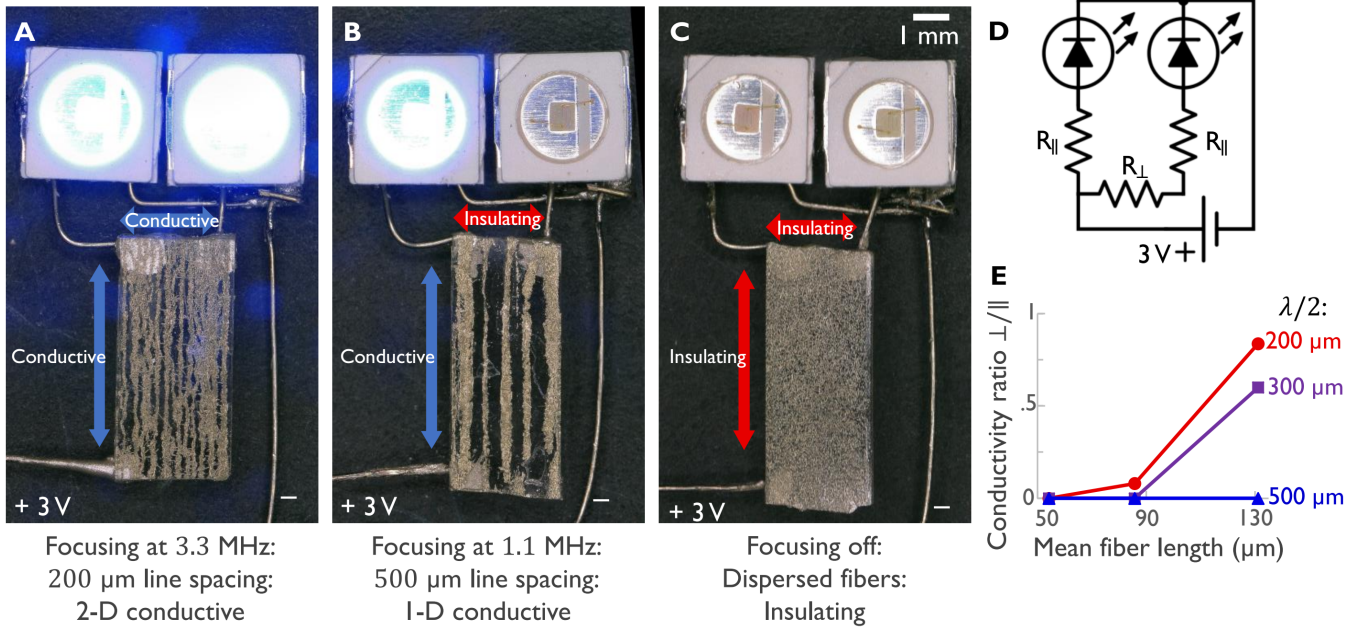


Figure 3: Three composites made using the same precursor ink: **A** An isotropic conductive 2.6% silver-coated glass fiber composite with focused bundle spacing ~ 200 μm completing a 3 V circuit to illuminate two 100 mA LEDs. Differences in LED brightness are due to tilt of the metallic reflector with respect to the camera. **B** An anisotropic conductive 2.6% silver-coated fiber composite with bundle spacing ~ 600 μm completing a 3 V circuit to illuminate only one 100 mA LEDs. **C** An insulating 2.6% silver-coated glass fiber composite made with acoustic focusing turned off. **D** Schematic of the circuit in A-C. **E** Transport anisotropy in 2.6% composites, given as the ratio of conductivity measured in the direction perpendicular to the focused lines to the that measured parallel.

We next demonstrate control of electrical transport anisotropy in patterned composites. Conductivity measurements reported above were reported parallel to the focused lines of carbon fibers. Modulating bundle spacing, however, controls fibers bridging behavior between bundles, which in turn controls the density of transport pathways in the perpendicular direction and anisotropy in conductivity. As shown in Fig. 4E, composites made with long fibers (mean length 130 μm) and close bundle spacing ($\lambda/2 \approx 200 \mu\text{m}$), are nearly-isotropic conductive materials, with conductivity measured in the direction perpendicular (\perp) to the focused lines 84% that measured in the parallel (\parallel) direction. At the widest spacing ($\sim 500 \mu\text{m}$), even using the longest fibers, bundles are insulated from each other in the perpendicular direction and the material is totally anisotropic. This fiber bridging behavior is explained by acoustics theory, as detailed in [SI]. By controlling the focused line spacing, the electric conductivity of the patterned composites can be modulated between anisotropic or nearly isotropic. This could be accomplished on-the-fly in a printing modality to give programmable spatial control of embedded electrical interconnects in a component.

To demonstrate the usefulness of modulating conductivity in highly conductive printable material with embedded interconnects, freestanding rigid composites were made with highly conductive particles. Silver-coated glass fibers impart conductivity $>5000 \text{ S/m}$ (10^5 S/m within assembled bundles, and 48% of the conductivity of bulk silver normalized to the volume of silver in the composites) to patterned composites. As a demonstration, a 2.6v% composite completes a circuit to supply an estimated 400 mA to 3 V LEDs in Fig. 3 without heat accumulation in ambient conditions. Anisotropy is modulated by choosing focusing frequencies that result in close spacing and fiber bridging, which results in nearly isotropic conductivity as in Fig. 3A, or wide spacing which results in anisotropic conductivity as in Fig. 3B. The composites made with the same precursor ink but without acoustic focusing, Fig. 3C, are insulating. Such high conductivity is typically accomplished only with post-printing polymer burn-off steps in conventional conductive material printing methods, since dispersed-particle composites require high filler volume fractions for high conductivity while printability requires low volume fractions [30, 31, 7]. This is ample current-carrying capacity for mm-scale soft-robotics applications, which typically require $<100 \text{ mA}$ for 1 N actuators [32, 33].

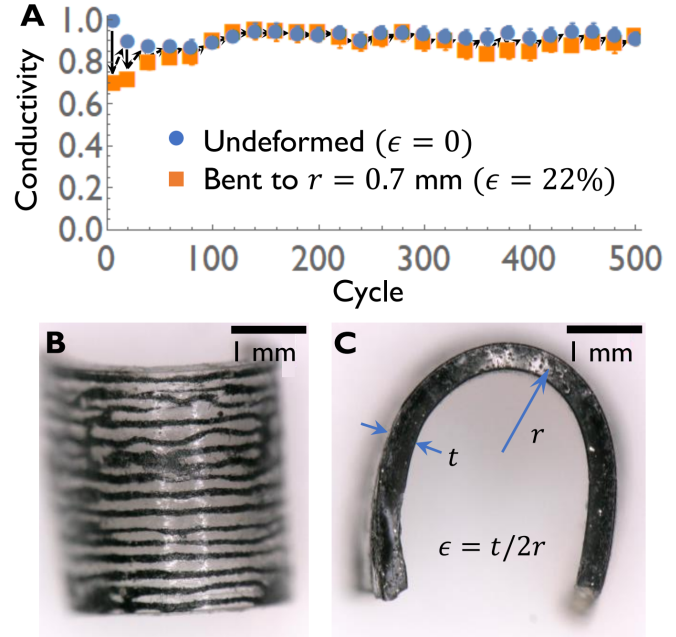


Figure 4: **A** Conductivity of elastomeric patterned composites after bending cycles to $\epsilon = t/2r = 22\%$, where $t = 300 \mu\text{m}$ is the composite thickness, as a fraction of pristine conductivity (34 S/m). **B,C** Micrographs of a 2.6% carbon-fiber elastomeric composite.

Next, to demonstrate the versatility and mechanical robustness of these focused fiber bundles, which is important in applications like soft robotics where highly conductive interconnects with strain tolerance is required, flexible patterned composites were made with carbon fibers in an elastomeric matrix (1:1 methyl:cyclo hexyl acrylate + 2wt% butanediol diacrylate, glass transition temperature $\approx 14.5^\circ\text{C}$). Conductivity values in the undeformed state are unchanged, but the composites are flexible. In a bending test, cycling between $\epsilon = 22\%$ (mandrel diameter 1.34 mm; tension) and $\epsilon = 0\%$ at a rate of $\sim 0.5 \text{ Hz}$ yielded nearly constant conductivity over 500 cycles, with conductivity recovering to $\sim 90\%$ of the undeformed value (34 S/m) in each cycle. This durability is due to the confinement of jammed, stiff conductive particles joined by freely rotating and sliding contacts within a deformable matrix, in contrast to conventional silver conductive inks which rely on loosely bound silver or graphene micro-flakes that exhibit large (20-600%) changes in conductivity with bending strain and roughly linear conductivity losses over multiple cycles [34, 35, 36]. Elastomer formulations with lower glass transition temperature or lower cross-linking density resulted in slower recovery times and lower cyclic durability.

In summary, acoustic focusing has been used to pattern the microstructure of printable composites and thereby modulate their material properties on the fly. Modulating acoustic assembly parameters allows production of composites from the same precursor ink which are

either insulating, isotropically conductive, or conductive in only one direction. Conductivity reaches values of 10^5 S/m within assembled structures, owing to close inter-particle contacts, at more than an order of magnitude lower fiber volume fractions than dispersed-fiber composites. Elastomeric composites have durable conductivity over at least 500 bending cycles to 0.7 mm radius.

Acoustic assembly of particle structures is naturally amenable to integration with 3D printing techniques. The device design and assembly dynamics are on the same scale as direct ink writing, where a nozzle is used for extrusion and deposition onto a substrate. The time required for particle assembly will allow printing at >1 mm/s substrate speeds, with little expected change in focused pattern continuity [21]. Low fiber volume fractions are required to produce conductive materials, alleviating clogging concerns during printing. Form-holding can be accomplished with shear-thinning additives [37] and partial UV-curing [38]. This versatile technology could pave the way for printing soft components with integrated electrical interconnects, possibly in addition to other integrated functionalities since the conditions for conductivity are lenient. Acoustic focusing's material agnostic nature encourages extension to other applications as well, such as thermal management materials, mass/ion transport materials, electroactive materials, and many others.

Acknowledgements

This work was supported by the Institute for Collaborative Biotechnologies through contract no. W911NF-09-D-0001 from the U.S. Army Research Office. The work used the Microfluidics Laboratory at the California Nanosystems Institute. The authors acknowledge Chris Bates and Craig Hawker for fruitful discussions.

References

- [1] E. MacDonald, R. Wicker, *Science* **2016**, *353*, 2093.
- [2] D. Rus, M. T. Tolley, *Nature* **2015**, *521*, 467–475.
- [3] A. D. Valentine, T. A. Busbee, J. W. Boley, J. R. Raney, A. Chortos, A. Kotikian, J. D. Berrigan, M. F. Durstock, J. A. Lewis, *Advanced Materials* **2017**, *29*, 1703817.
- [4] J. Chen, X. Huang, Y. Zhu, P. Jiang, *Advanced Functional Materials* **2017**, *27*, 1604754.
- [5] B. G. Compton, J. A. Lewis, *Advanced Materials* **2014**, *26*, 5930–5935.
- [6] J. N. Coleman, U. Khan, Y. K. Gun'ko, *Advanced Materials* **2006**, *18*, 689–706.
- [7] B. Y. Ahn, E. B. Duoss, M. J. Motala, X. Guo, S.-I. Park, Y. Xiong, J. Yoon, R. G. Nuzzo, J. A. Rogers, J. A. Lewis, *Science* **2009**, *323*, 1590–1593.
- [8] C. Xia, A. C. Garcia, S. Q. Shi, Y. Qiu, N. Warner, Y. Wu, L. Cai, H. R. Rizvi, N. A. D'Souza, X. Nie, *Scientific Reports* **2016**, *6*,.
- [9] R. R. Collino, T. R. Ray, R. C. Fleming, J. D. Cornell, B. G. Compton, M. R. Begley, *Extreme Mechanics Letters* **2016**, *8*, 96–106.
- [10] R. L. Truby, J. A. Lewis, *Nature* **2016**, *540*, 371–378.
- [11] B. Derby, *Annual Review of Materials Research* **2010**, *40*, 395–414.
- [12] M. L. Shofner, K. Lozano, F. J. Rodríguez-Macías, E. V. Barrera, *Journal of Applied Polymer Science* **2003**, *89*, 3081–3090.
- [13] F. Ning, W. Cong, J. Qiu, J. Wei, S. Wang, *Composites Part B: Engineering* **2015**, *80*, 369–378.
- [14] H. L. Tekinalp, V. Kunc, G. M. Velez-Garcia, C. E. Duty, L. J. Love, A. K. Naskar, C. A. Blue, S. Ozcan, *Composites Science and Technology* **2014**, *105*, 144–150.
- [15] J. Greenhall, F. Guevara Vasquez, B. Raeymaekers, *Applied Physics Letters* **2016**, *108*, 103103.
- [16] J. Greenhall, B. Raeymaekers, *Advanced Materials Technologies* **2017**, *2*, 1700122.
- [17] D. Kokkinis, M. Schaffner, A. R. Studart, *Nature Communications* **2015**, *6*,.
- [18] J. J. Martin, B. E. Fiore, R. M. Erb, *Nature Communications* **2015**, *6*,.
- [19] E. Loth, S. Baumann, C. P. Lutz, D. M. Eigler, S. Heinrich, *Science* **2012**, *335*, 196–199.
- [20] J. P. Lewicki, J. N. Rodriguez, C. Zhu, M. A. Worsley, A. S. Wu, Y. Kanarska, J. D. Horn, E. B. Duoss, J. M. Ortega, W. Elmer, R. Hensleigh, R. A. Fellini, M. J. King, *Scientific Reports* **2017**, *7*,.
- [21] R. R. Collino, T. R. Ray, L. M. Friedrich, J. D. Cornell, C. D. Meinhart, M. R. Begley, *Materials Research Letters* **2018**, *6*, 191–198.
- [22] J. Greenhall, F. Guevara Vasquez, B. Raeymaekers, *Applied Physics Letters* **2014**, *105*, 144105.
- [23] S. M. Hagsäter, T. G. Jensen, H. Bruus, J. P. Kutter, *Lab on a Chip* **2007**, *7*, 1336.
- [24] R. R. Collino, T. R. Ray, R. C. Fleming, C. H. Sasaki, H. Haj-Hariri, M. R. Begley, *Extreme Mechanics Letters* **2015**, *5*, 37–46.
- [25] L. V. King, *Proceedings of the Royal Society A: Mathematical Physical and Engineering Sciences* **1934**, *147*, 212–240.
- [26] L. P. GOR'KOV, *Sov. Phys. Dokl.* **1962**, *6*, 773–775.
- [27] H. Bruus, *Lab on a Chip* **2012**, *12*, 1014.
- [28] R. M. Mutiso, K. I. Winey, *Progress in Polymer Science* **2015**, *40*, 63–84.
- [29] M. Foygel, R. D. Morris, D. Anez, S. French, V. L. Sobolev, *Physical Review B* **2005**, *71*,.
- [30] A. C. de Leon, B. J. Rodier, C. Bajamundi, A. Espera, P. Wei, J. G. Kwon, J. Williams, F. Ilijasic, R. C. Advincula, E. Pentzer, *ACS Applied Energy Materials* **2018**, *1*, 1726–1733.

- [31] G. Postiglione, G. Natale, G. Griffini, M. Levi, S. Turri, *Composites Part A: Applied Science and Manufacturing* **2015**, *76*, 110–114.
- [32] T. Levard, P. J. Diglio, S.-G. Lu, C. D. Rahn, Q. M. Zhang, *Smart Materials and Structures* **2012**, *21*, 012001.
- [33] M. T. Cortés, J. C. Moreno, *e-Polymers* **2003**, *3*,.
- [34] X. Z. Niu, S. L. Peng, L. Y. Liu, W. J. Wen, P. Sheng, *Advanced Materials* **2007**, *19*, 2682–2686.
- [35] K. S. Kim, Y. Zhao, H. Jang, S. Y. Lee, J. M. Kim, K. S. Kim, J.-H. Ahn, P. Kim, J.-Y. Choi, B. H. Hong, *Nature* **2009**, *457*, 706–710.
- [36] S. Merilampi, T. Björninen, V. Haukka, P. Ruuskanen, L. Ukkonen, L. Sydänheimo, *Microelectronics Reliability* **2010**, *50*, 2001–2011.
- [37] L. Friedrich, R. Collino, T. Ray, M. Begley, *Sensors and Actuators A: Physical* **2017**, *268*, 213–221.
- [38] R. D. Farahani, L. L. Lebel, D. Therriault, *Journal of Micromechanics and Microengineering* **2014**, *24*, 055020.